Nanoelectronics and Its New Materials – A NEW ERA OF NANOSCIENCE

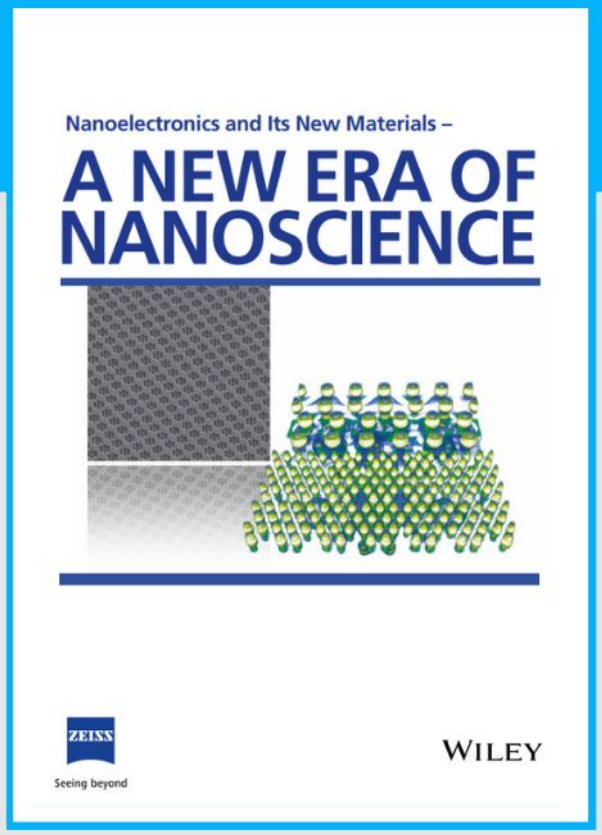

Discover the recent advances in electronics research and fundamental nanoscience.

Nanotechnology has become the driving force behind breakthroughs in engineering, materials science, physics, chemistry, and biological sciences. In this compendium, we delve into a wide range of novel applications that highlight recent advances in electronics research and fundamental nanoscience. From surface analysis and defect detection to tailored optical functionality and transparent nanowire electrodes, this eBook covers key topics that will revolutionize the future of electronics.

To get your hands on this valuable resource and unleash the power of nanotechnology, simply download the eBook now. Stay ahead of the curve and embrace the future of electronics with nanoscience as your guide.

ZEISS

Seeing beyond

WILEY

NANO · MICRO small

www.small-journal.com

Low Threshold Fabry–Pérot Mode Lasing from Lead Iodide Trapezoidal Nanoplatelets

Yangguang Zhong, Qi Wei, Zhen Liu, Qiuyu Shang, Liyun Zhao, Ruiwen Shao, Zhepeng Zhang, Jie Chen, Wenna Du, Chao Shen, Jun Zhang, Yanfeng Zhang, Peng Gao, Guichuan Xing, Xinfeng Liu,* and Qing Zhang**

Lead Iodide (PbI_2) is a layered semiconductor with direct band gap holding great promises in green light emission and detection devices. Recently, PbI_2 planar lasers are demonstrated using hexagonal whispering-gallery-mode microcavities, but the lasing threshold is quite high. In this work, lasing from vapor phase deposition derived PbI_2 trapezoidal nanoplatelets (NPs) with threshold that is at least an order of magnitude lower than the previous value is reported. The growth mechanism of the trapezoidal NPs is explored and attributed to the synergistic effects of van der Waals interactions and lattice mismatching. The lasing is enabled by the population inversion of $n = 1$ excitons and the optical feedback is provided by the Fabry–Pérot oscillation between the side facets of trapezoidal NPs. The findings not only advance the understanding of growth and photophysics mechanism of PbI_2 nanostructures but also provide ideas to develop low threshold ultrathin lasers.

Y. G. Zhong, Dr. Q. Wei
Key Laboratory of Flexible Electronics and Institute of Advanced Materials
Jiangsu National Synergetic Innovation Center for Advanced Materials
Nanjing Tech University
30 South Puzhu Road, Nanjing 211816, China

Y. G. Zhong, Dr. Q. Wei, Z. Liu, Q. Y. Shang, L. Y. Zhao, Z. P. Zhang, J. Chen, Prof. Y. F. Zhang, Prof. Q. Zhang
Department of Materials Science and Engineering
College of Engineering
Peking University
Beijing 100871, China
E-mail: Q_zhang@pku.edu.cn

Q. Y. Shang, Prof. Q. Zhang
Research Center for Wide Gap Semiconductor
Peking University
Beijing 100871, China

Dr. R. W. Shao, Prof. P. Gao
Electron Microscopy Laboratory
School of Physics
Peking University
Beijing 100871, China

Z. P. Zhang, Prof. Y. F. Zhang
Center for Nanochemistry
Beijing National Laboratory for Molecular Sciences
College of Chemistry and Molecular Engineering
Academy for Advanced Interdisciplinary Studies
Beijing National Laboratory for Molecular Sciences
College of Chemistry and Molecular Engineering
Peking University
Beijing 100871, China

J. Chen, Dr. W. N. Du, Prof. X. F. Liu
Division of Nanophotonics
CAS Key Laboratory of Standardization and Measurement for Nanotechnology
CAS Center for Excellence in Nanoscience
National Center for Nanoscience and Technology
Beijing 100190, China
E-mail: Liuxf@nanoctr.cn

Prof. C. Shen, Prof. J. Zhang
State Key Laboratory of Superlattices and Microstructures
Institute of Semiconductors
Chinese Academy of Sciences
Beijing 100083, China

Prof. C. Shen, Prof. J. Zhang
College of Materials Science and Opto-Electronic Technology
University of Chinese Academy of Sciences
Beijing 100049, China

Prof. P. Gao
International Center for Quantum Materials
School of Physics
Peking University
Beijing 100871, China

Prof. P. Gao
Collaborative Innovation Center of Quantum Matter
Beijing 100871, China

Prof. G. C. Xing
Joint Key Laboratory of the Ministry of Education
Institute of Applied Physics and Materials Engineering
University of Macau
Avenida da Universidade
Taipa, Macao, SAR 999078, China
E-mail: gcxing@umac.mo

The ORCID identification number(s) for the author(s) of this article can be found under https://doi.org/10.1002/smll.201801938.

DOI: 10.1002/smll.201801938

two-dimensional (2D) layered semiconductors are important for the development of ultrathin and stretchable optoelectronics due to their atomic-level thickness, nondangling bonds surface and novel spin and exciton properties defined by strong quantum effects, etc.[1–7] Solid-state planar lasers using 2D semiconductor as gain media can be easily integrated onto heterogeneous substrates and promises for chip-level light sources.[8–13] Due to the absence of surface dangling bonds, 2D semiconductors lasers can maintain good device performance for long lifetime even in few atomic layer levels.[14,15] The enhanced Coulomb interaction of 2D semiconductors not only effectively enhances intrinsic differential gain, but also ensures high exciton oscillation strength to realize low threshold exciton–polariton laser.[16,17]

So far, considerable efforts have been made in 2D semiconductor lasers.[18–20] However, most of these 2D lasers have adopted monolayer transition metal dichalcogenides, which in turn brings great challenge to gain and cavity fabrications due to the lack of self-confined cavity and the limit of optical gain volume.[21] Compared with the transition metal dichalcogenides those exhibit direct to indirect band gap transition from monolayer to multilayer, lead iodide (PbI_2) is a layered semiconductors with direct band gap from monolayer to bulk phase, and hence holds great promises in 2D emission devices.[22–25] Meanwhile, PbI_2 is heavy ionic polar semiconductor of great fundamental interests owing to strong exciton–phonon interaction. Also, the heavy atoms component Pb and I make PbI_2 potential for radiation detectors.[26–28] Furthermore, PbI_2 is a precusor of organic–inorganic and all-inorganic lead halide perovskites which have recently attracted great attentions in low threshold lasers.[29–35] The study of PbI_2 laser will be helpful to understand the photophysics of perovskite lasing. Pioneer studies have been made on lasing from individual PbI_2 nanostructures fabricated by solution processed or vapor phase deposition (CVD) methods.[36,37] However, the lasing threshold is quite high (≈200 μJ cm^{-2}) even at low temperature of ≈77 K, which hinders the potential applications of PbI_2 laser in ambient condition. Therefore, it is urgent to explore new structures of PbI_2 microcavities with lower lasing threshold toward practical applications.

In this work, we have addressed the synthesis of 2H-polytype PbI_2 trapezoidal nanoplatelets (NPs) on mica substrate. The trapezoidal NP is vertically aligned on the mica substrate with growth direction of [110] via the synergistic effects of van der Waals (vdW) interactions and lattice mismatching. Optically pumped lasing is achieved from the trapezoidal NPs with the threshold of 126.2 μJ cm^{-2} at 200 K and 44.5 μJ cm^{-2} at 120 K, which is one order lower than those reported in Fabry–Pérot (FP) and whispering-gallery-mode (WGM) microcavities previously. Lasing mechanism is further unveiled by mode simulations, low temperature and time-resolved photoluminescence (TRPL) spectroscopy. These results push forward the applications research of 2D lasers and advance fundamental understanding of growth mechanism and photophysics of lead halide and related material systems.

Figure 1a shows the 2H-polytype PbI_2 structure, in which the Pb atoms are surrounded by six I atoms and then forms an octahedral $[PbI_6]^{4-}$ unit. The $[PbI_6]^{4-}$ layers is bounded by weak vdW interactions with separation of 0.698 nm.[38] In general, the unit cell of PbI_2 contains one Pb atom and two I atoms, where Pb atom occupies the top corner and I atoms locate at quarter positions in the lattice (Figure S1, Supporting Information). Figure 1b shows typical scanning electron microscopy of

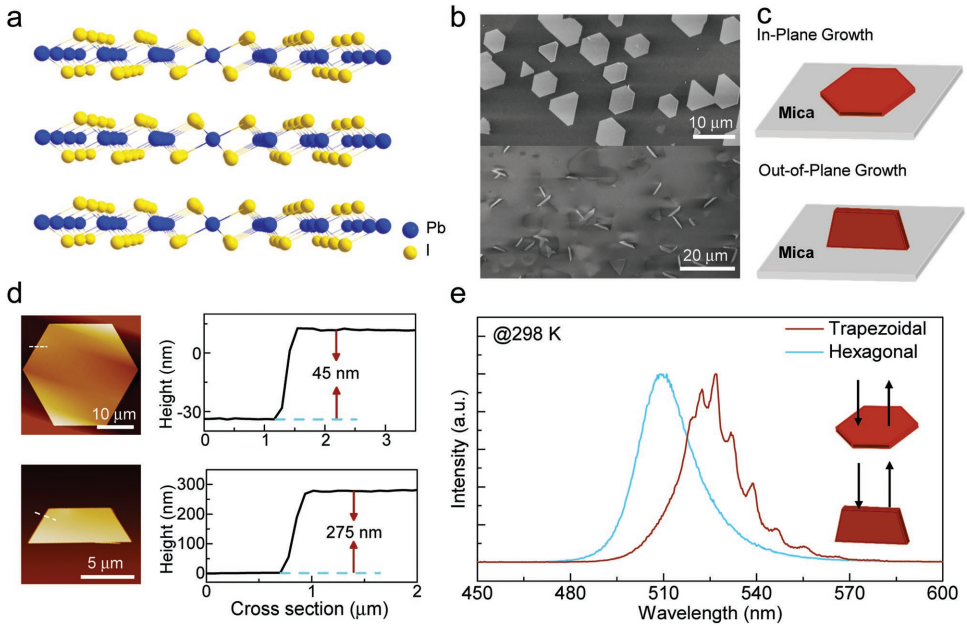

Figure 1. Lead iodide nanoplatelets (NPs) grown on mica substrate via chemical vapor deposition (CVD) method. a) Lattice structure of 2H-PbI_2. b) Scanning electron microscope (SEM) image of in-plane-epitaxial hexagonal NPs (upper plane) and out-of-plane-epitaxial trapezoidal NPs (lower plane) on mica. c) The corresponding growth diagram of in-plane-epitaxial hexagonal NPs (upper plane) and out-of-plane-epitaxial trapezoidal NPs (lower plane). d) Atomic force microscope (AFM) images of an in-plane-epitaxial hexagonal NP (upper) and an out-of-plane-epitaxial NP (lower). The surface roughness: 0.28 nm for hexagonal NP; 0.52 nm for trapezoidal NP. e) Room-temperature PL spectra of typical in-plane-epitaxial hexagonal NP (ocean blue line) and out-of-plane-epitaxial trapezoidal NP (sunset red line). Inset: the schematic diagram of excitation and collection configuration.

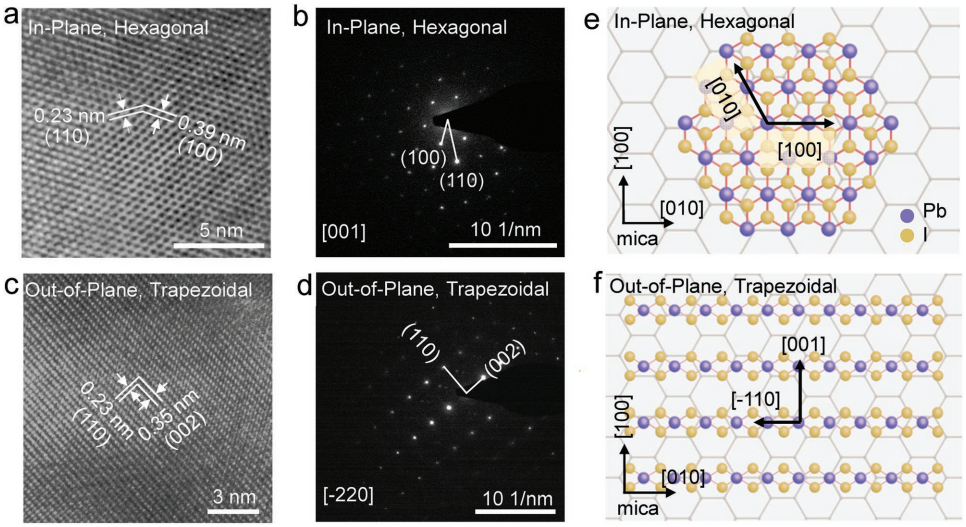

Figure 2. a) HRTEM image of the in-plane-epitaxial hexagonal NPs, ≈0.39 nm and ≈0.23 nm are correlated to the (100) and (110) plane, respectively. The scale bar is 5 nm. b) The SAED is taken along [001] direction from (a). c) HRTEM image of the out-of-plane-epitaxial trapezoidal NPs, 0.35 and 0.23 nm are correlated to the (002) and (110) plane, respectively. The scale bar is 3 nm. d) The SAED is taken along [–220] direction from (c). e) Schematic illustration of the vdW epitaxy of the in-plane-epitaxial hexagonal NPs. The nucleation preferentially occurs in the low energy surface (001) and stacks layer by layer along [001] direction. The growth rate along the lateral directions [100] and [010] is much faster than the vertical direction [001]. f) Top view of incommensurate epitaxial growth of out-of-plane-epitaxial trapezoidal PbI_2 NPs. The NPs are stacking along [110] direction of PbI_2 and perpendicular to mica surface of (001). The lattice matches models are shown: $9 \times d_{PbI2(-220)} \approx 2 \times d_{mica(010)}$ (i.e., that $9 \times d_{PbI2(-110)} \approx 4 \times d_{mica(010)}$) and $3 \times d_{PbI2(002)} \approx 2 \times d_{mica(100)}$ (i.e., that $3 \times d_{PbI2(001)} \approx 4 \times d_{mica(010)}$). The f values of PbI_2 [–220]//mica [010] and PbI_2 [002]//mica [100] are 1.5% and –0.67%, respectively.

the as-fabricated NPs on the muscovite mica by CVD methods using PbI_2 powders as source (Figure S2, Supporting Information).[39,40] The NPs can be divided into two types according to the epitaxial direction: aligned parallel (in-plane, upper panel) and vertical to (out-of-plane, bottom panel) the mica surface. The in-plane-epitaxial NPs exhibit triangle and hexagonal shapes which have been reported in the previous literatures;[37] while the out-of-plane-epitaxial NPs are trapezoidal in shape. The statistical histogram suggests that the trapezoidal NPs distribute along three directions correlate to [100], [1-10], and [-1-10] of mica substrate, respectively (Figure S3, Supporting Information). Figure 1c shows the corresponding growth diagram of in-plane-epitaxial hexagonal NPs (upper plane) and out-of-plane-epitaxial trapezoidal NPs (lower plane). Figure 1d displays the atomic force microscopy images of the in-plane hexagonal and out-of-plane-epitaxial trapezoidal NPs. The root-mean-square roughness of the hexagonal and the trapezoidal NPs are 0.28 and 0.52 nm, respectively, which are perfectly smooth in optical level. Figure 1e displays the room-temperature PL spectra of hexagonal and trapezoidal NPs respectively. The schematic diagram of excitation and collection configuration is shown in the inset of Figure 1e. The PL spectra of hexagonal NPs which can be well fitted by the sum of two Lorentzian functions centered at ≈507 and ≈516 nm, respectively (Figure S4, Supporting Information). The origin of the two emission peaks will be discussed in the following sections. Compared with the hexagonal NPs, the PL spectra of trapezoidal NPs show slight redshifts possibly owing to the self-absorption effect considering the longer light propagation distance in the reflective mode excitation and collection geometry of optical measurement system.[41] Notably, a group of sharp peaks with full width at half maximum (FWHM) of ≈2.8–8.4 nm appear in the lower energy side of PL for the trapezoidal NPs. The spacing between the two adjacent oscillation peaks becomes smaller in the larger NPs and nearly inversely proportional to the circumference of the NPs, indicating that the sharp peaks are the resonant modes of an optical cavity defined in the NPs (Figures S5–S7, Supporting Information) and also good quality of the as-formed microcavities.

High-resolution transmission electron microscopy (HRTEM) is performed to study the crystalline structures and growth mechanisms of the NPs, as shown in **Figure 2**. The HRTEM image of the hexagonal NPs (Figure 2a) shows hexagonal lattice with plane distances of ≈0.39 and ≈0.23 nm those match well with the lattice spacing of the (100) and (110) planes of 2H-PbI_2 (PDF No. 7-235), respectively. The corresponding selected-area electron diffraction (SAED) pattern NPs (Figure 2b) confirms that the intersection angle of the two planes (100) and (110) is 30°. The results suggest that the hexagonal NPs are stacked along the [001] direction of PbI_2.[42] Figure 2c,d presents the HRTEM image and corresponding SAED of the transferred trapezoidal NPs, respectively. The lattice fringe with distances of ≈0.35 nm is correlated to the (002) plane, while lattice spacing of ≈0.23 nm is indexed to the (110) plane. The SAED pattern further reveals that the interplane angle is exactly 90°, which coincides with the TEM image. The [-220] crystal zone axis of the trapezoidal NPs suggests a different growth kinetics compared with the hexagonal NPs. Temperature-dependent and polarization dependent Raman spectroscopy is conducted to further study the phase structure of these PbI_2 NPs (Figure S8, Note 1, Supporting Information). The Raman spectra of both NPs exhibits strong peaks corresponding to phonon modes of E_g (72 cm^{-1}), A_{1g} (95 cm^{-1}), and A_{2u} (110 cm^{-1}), suggesting that the NPs have the same crystalline structure. The appearance

of high-order Raman modes $E_g + A_{1g}$ (166 cm^{-1}) and $2A_{2u}$ (214 cm^{-1}) suggests a strong electron–phonon coupling because of polar Frölich interaction.[43,44] A frequency Davydov splitting at 72 cm^{-1}, expected in 4H-PbI_2, is not observed in the as-grown NPs, strongly supporting that the crystalline structures of NPs are 2H-polytype.[45] The polarization resolved Raman spectra are good consistent with the TEM data (Note 1, Supporting Information). Figure 2e shows schematic illustration of the vdW epitaxy of the in-plane-epitaxial hexagonal NPs. The nucleation preferentially occurs in the low energy surface (001) and stacks layer by layer along [001] direction. The growth rate along the lateral directions [100] and [010] is much faster than the vertical direction [001]. And Figure 2f shows the top view of incommensurate epitaxial growth of out-of-plane-epitaxial trapezoidal PbI_2 NPs. The NPs are stacking along [110] direction of PbI_2 and perpendicular to mica surface of (001).

The nucleation growth mechanisms of PbI_2 nanostructures on mica substrates are discussed. During the vapor–solid synthesis process,[46] the probability of 2D nucleation on the surface of a whisker, F_n, can be described as[47]

$$F_n = A \exp\left(-\frac{\pi\sigma^2}{k^2T^2 \ln\alpha}\right) \quad (1)$$

Here, A is a constant, σ is the surface energy, T is the temperature, α is the ratio of actual pressure to equilibrium vapor pressure, so-called supersaturation ratio. According to the equation, the surface energy is essential that the smaller surface energy, the higher the 2D nucleation probability.[48] The hexagonal PbI_2 NPs is exactly grown from 2D nuclei along the direction of [001] on the layered mica substrates.[42,49–52] The 2D nucleation growth is owing to: 1) the theoretical energy of (001) plane is the lowest (0.428 J m^{-1}) and hence the F_n is the highest among the lattice planes of PbI_2;[42] 2) the interactions between the mica substrate and the basal plane (001) with hexagonal closed-packed lattice further promotes the 2D nucleation in the low energy surface.[47]

In the growth process of vertically aligned trapezoidal NPs, the lattice matching between mica and PbI_2 becomes more predominant. According to the HRTEM image, the PbI_2 trapezoidal NPs grow either along (002) or (110) plane on the (001) plane of mica substrate. Both the two planes of PbI_2 have quite large lattice mismatch with mica substrate. Considering that the mismatch is relatively lower for the (002) plane (in Table S1, Supporting Information), two incommensurate epitaxial models are proposed: (i) PbI_2 [-220]//mica [010] and PbI_2 [002]//mica [100]; (ii) PbI_2 [002]//mica [010] and PbI_2 [-220]//mica [100]. The plane distances are $d_{PbI2(002)}$ = 3.49 Å, $d_{PbI2(-220)}$ = 1.97 Å, $d_{mica(100)}$ = 5.20 Å, and $d_{mica\ (010)}$ = 9.00 Å.[53,54] The lattice match models and the mismatch values f, expressed as $f = (1\text{-}d_{PbI2}/d_{mica}) \times 100\%$, are shown as below

(i) $9 \times d_{PbI2(-220)} \approx 2 \times d_{mica(010)}$ (i.e., that $9 \times d_{PbI2(-110)} \approx 4 \times d_{mica(010)}$) and $3 \times d_{PbI2(002)} \approx 2 \times d_{mica(100)}$ (i.e., that $3 \times d_{PbI2(001)} \approx 4 \times d_{mica(010)}$). The f values of the two directions are 1.5% and –0.67%, respectively.

(ii) $5 \times d_{PbI2(-220)} \approx 2 \times d_{mica(100)}$ and $8 \times d_{PbI2(002)} \approx 3 \times d_{mica(010)}$. The corresponding f values for the two directions are –3.3% and 5.6%, respectively.

The model (i) is preferred on the basis of lowest lattice match. Further, since the lattice mismatch along the direction of PbI_2 [002]//mica [100] (–0.67%) is lower than that of PbI_2 [–220]// mica [010] (1.5%), the growth rate [002] direction is much faster than that of [–220], leading to 1D anisotropy growth in (002) plane. The growth of the trapezoidal NPs is a 3D nucleation process likely to occurring at small F_n. Considering the absence of lowest energy surface (001) plane in these NPs, the temperature and supersaturation ratio become two predominant factors for the morphology control. In the other words, the growth of the trapezoidal NPs is expected at relatively lower temperature, or with the decreasing of actual vapor pressure after a period of reaction.

Next, the lasing properties of the trapezoidal NPs are explored. As shown in **Figure 3**a, an individual trapezoidal NP is optically pumped by 400 nm femtosecond laser pulses at 200 K. Under low pump fluence (P = 87.5 μJ cm^{-2}), a broad spontaneous emission band centered at 513 nm with a FWHM of λ_{FWHM} = 14 nm can be observed. As the pump fluence approaches ≈126.2 μJ cm^{-2}, a sharp peak centered at around 516 nm appears with FWHM of 0.4 nm at the red side of the main spontaneous emission peak. When the pump fluence further increases to P > 143.7 μJ cm^{-2}, more narrow peaks emerge with intensities increasing much faster than the spontaneous emission background. Figure 3b shows the light emission intensity (right axis) and the FWHM (left axis) as a function of pump fluence, respectively. The evolution of PL spectra exhibits a concurrent sharp decreasing in FWHM and spiraling upward of light input–output at the lasing threshold. The linewidth narrowing and superlinear intensity increase above the threshold P_{th} = 126.2 μJ cm^{-2}, confirming the occurrence of lasing. The optical image of the trapezoidal NP above the lasing threshold (inset, Figure 3b) shows that the bright lasing emissions are mainly coupled out at the two lateral edges of the trapezoid NPs, preliminarily suggesting that optical feedback in the trapezoidal NPs comes from the FP oscillation between the two lateral facets. The free spectra range (FSR), $\Delta\lambda$ at resonance mode of λ can be described by $\Delta\lambda = \lambda^2/2Ln_g$, where n_g is the group refractive index, L is the cavity length.[55] The FSR is linear to the inverse of cavity length (Figure S9, Supporting Information), and a group refractive index n_g of ≈5.16 is extracted out using the linear relation equation, which agrees well with previous studies.[50] Finite-differential time-domain simulation has been utilized to further analyze the optical mode and calculate electric fields distribution inside trapezoidal NP microcavity (Figure 3c). The optical field is well confined inside the microcavity and reflected between the two side facets and base facet (as the red line shown) of the trapezoidal NP. Due to the good confinement of the NP, the optical field can only be coupled out from the side facets and base facets, which coincides with the PL images above the lasing threshold (Figure 3b, inset).

Temperature-dependent PL spectroscopy is conducted below and above lasing threshold to explore the lasing mechanism of the trapezoidal NPs. The temperature varies from 230 to 120 K. As shown in **Figure 4**a, the emission spectroscopy can be decomposed into two Lorenz peaks indicated as X_1 (lower energy, 509 nm, 2.43 eV, at 200 K) and X_2 (higher energy, 499.8 nm, 2.48 eV at 200 K). Both peaks exhibit blueshift and the FWHM becomes smaller with the decreasing

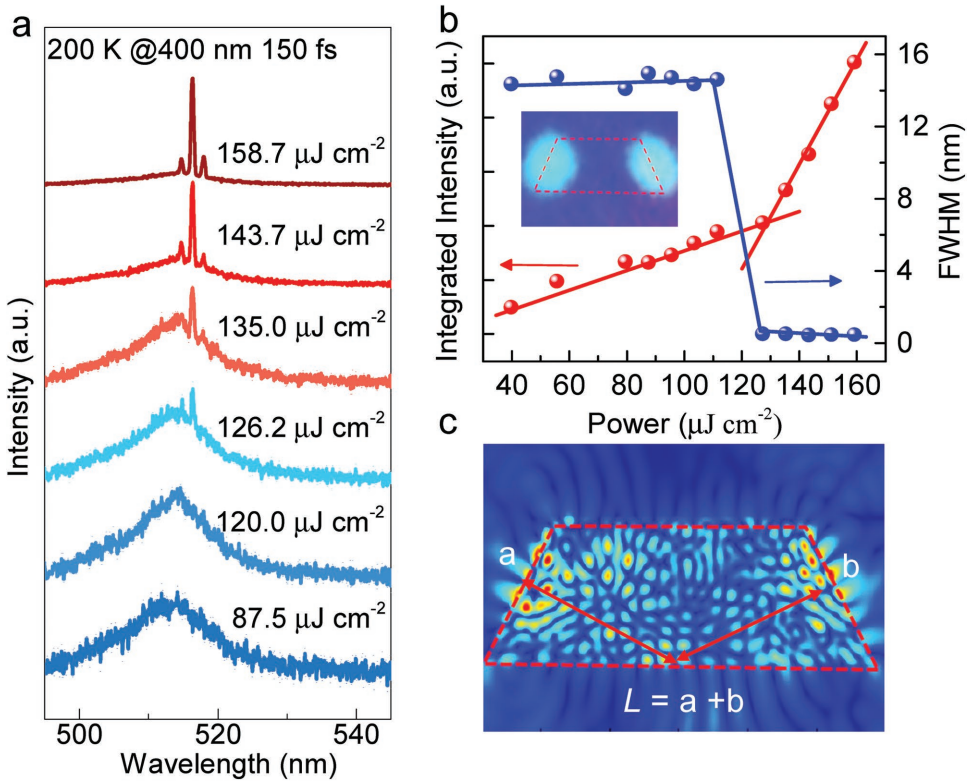

Figure 3. Lasing from out-of-plane-epitaxial trapezoidal PbI_2 NPs at 200 K. a) The evolution spectroscopy from spontaneous emission to lasing status; the pumping fluence increases from 87.5 to 158.7 μJ cm^{-2}; the spacing between the adjacent modes is ≈1.6 nm; the short edge length and the long edge length of the sample are 4 and 6 μm, respectively. b) The power-dependent of the integrated intensity and FWHM of lasing mode at 516.3 nm. The threshold is ≈126.2 μJ cm^{-2}. Inset: PL image above threshold. c) Simulated electric field distribution at 510 nm. The electric fields are well confined at the two side facets of the trapezoidal NP. The light propagation pathway *L* is described by red arrow line.

of temperature owing to the lattice shrink and lower phonon scattering, respectively.[56] The origins of the two peaks could be contributed from the recombination of either free, bound, multiple, or charged excitons. The high energy emission X_2 was generally attributed to free excitons recombination.[23,57–59] However, the origin of low energy emission X_1, are controversial that the peak is either assigned to free-to-bound transition related with defects or second order exciton.[37,60,61] Power-dependent PL spectroscopy is a well-established method to probe the recombination mechanism of emission peak. The power law k of free exciton and free-to-bound recombination intensity is ≈1–1.3 and 0–1, respectively.[62] As shown in Figure 4b and Figure S10, k is 1.1–1.3 for both X_1 and X_2 peaks, which accords with the emission of free exciton. After increasing of defect density through sample degeneration, the intensity ratio of X_1 and X_2 do not change, confirming that the origin of the X_1 peak is not related with defects (Figure S11, Supporting Information). In the layered semiconductors, high order excitons are widely observed owing the strong quantum confinement effect.[63] Here the energy of X_1 and X_2 are ≈2.46 and 2.49 eV are close to those of n = 1 and n = 2 excitons reported previously.[64] The energy difference between the two excitons reduces with the decreasing of temperature, which coincides with the decreasing of exciton effective mass owing to the less population of phonons interacting with excitons.[65–67] Therefore we assign the X_1 and X_2 to the recombination of n = 1 and n = 2 excitons, respectively.[68] Figure 4c displays temperature-dependent lasing spectra with T = 120–180 K. It can be seen that the lasing peaks always locate in the spectra range of X_1, suggesting that the lasing is due to the population inversion of n = 1 excitons. Figure 4d shows the plots of lasing threshold versus temperature. With the decreasing of temperature from 200 to 120 K, the lasing threshold decreases from 126.2 to 44.5 μJ cm^{-2}. The increments of lasing threshold at higher temperature are mainly caused by thermal-activated nonradiative processes, in which the lasing threshold is described as $P_{th} = P_{th,0}\exp(T/T_0 - 1)$.[69] T_0 is so-called characteristic temperature and a critical parameter to evaluate the thermal stability of lasing devices. The T_0 is extracted to be 81 K, which is relatively lower than those of ZnO (90–130 K) and GaN (160–246 K).[70,71] Nevertheless, the characteristic temperature of as-grown trapezoidal NPs is larger than that of hexagonal PbI_2 NP (45 K), which coincides with the lower threshold in the trapezoidal NPs.[37] Overall, as shown in Table S2 of the Supporting Information, the lasing threshold of the trapezoidal NPs at 120 K (44.5 μJ cm^{-2}) is nearly two orders lower than the values in PbI_2 microlasers operated at 77 K (200 μJ cm^{-2}) reported previously, strongly suggesting the high quality of the as-grown PbI_2 trapezoidal FP microcavities.[37,72,73]

In the hexagonal NPs, WGM mode lasing is achieved (Figure S12, Supporting Information), but the threshold (≈2.3 × 10^3 μJ cm^{-2} at 200 K and ≈1.1 × 10^3 μJ cm^{-2} at 180 K)

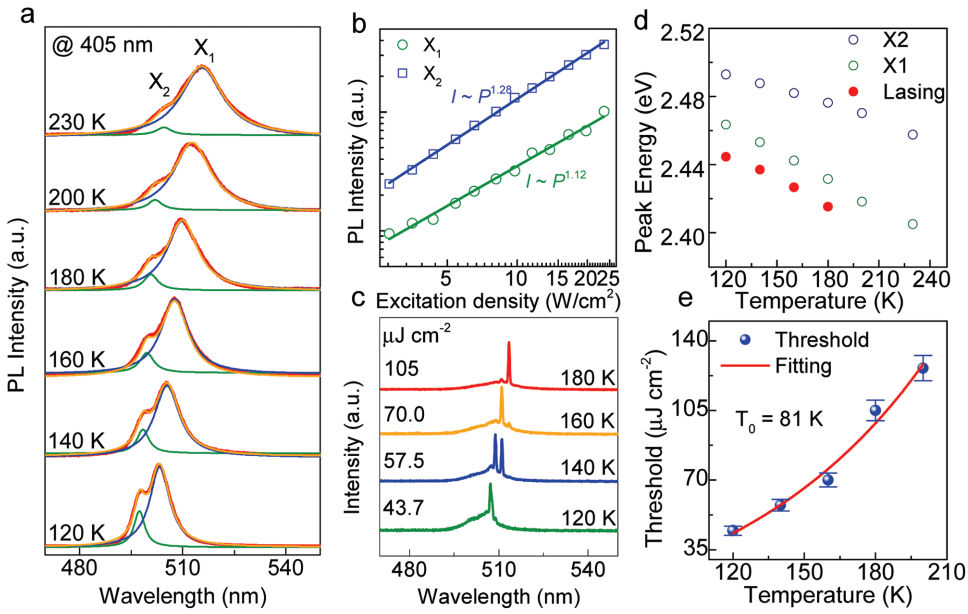

Figure 4. Temperature-dependent spontaneous emission and lasing spectra of out-of-plane-epitaxial trapezoidal PbI_2 NPs. The lengths of short edge and the long edge of the NP are 3.8 and 5.1 μm, respectively. a) Spontaneous emission spectra with temperature varying from 120 to 230 K. b) Power-dependent spontaneous emission intensity of X_1 and X_2 peaks, which are fitted by the function of $I \propto P^{\alpha}$. c) Temperature-dependent lasing spectra. d) The temperature dependence of X_1, X_2, and lasing energy. e) Lasing thresholds as a function of temperature. Dots: the threshold with the error bar; red lines: fitting curve using equation of $P_{th} = P_{th,0}\exp(T/T_0 - 1)$. T_0 is estimated to 81 K.

is much higher than the trapezoidal NPs, which demonstrates a good merit of the trapezoidal NPs. Herein, the lasing thresholds of groups of trapezoidal and hexagonal NPs are compared at 200 K, as shown in **Figure 5**a. The lasing thresholds of the hexagonal NPs are ≈0.7–2.7 × 10^3 μJ cm^{-2}, which is one order higher than those of their trapezoidal counterparts (≈41–137.5 μJ cm^{-2}) with similar dimension. For the semiconductor cavities, the optical losses are mainly induced by the radiation loss at the non-100% reflective end-facets and the nonradiative processes owing to defect states, Auger recombination, etc.[74,75] For the WGM mode of hexagonal NP, the reflection of the six end-facets can be nearly regarded as the total reflection with little radiation loss. As a contrast, the reflectivity of FP mode in trapezoidal NP is only 37%, leading to a round-trip loss of 86%, which is much higher than the hexagonal NP. The lower threshold of trapezoidal NP is benefited from the higher crystalline quality and lower density of trapping states. Considering the lattice of mica surface is not perfect, which contains unreleased strain and impurities including structure defects, adsorbate, etc., which will introduce defects in PbI_2 grown on it. The trapezoidal NPs are vertically grown on the mica with smaller contact area than the hexagonal NPs, which can reduce the influence of these impurities and therefore show the better crystalline quality. The lower density of defects in the trapezoidal NPs is proven by PL and TRPL and the absorption spectroscopy. As shown in Figure 5b, the PL intensity of trapezoidal NPs (thickness: 175 nm) is five times higher than that of the hexagonal NPs with the same thickness, which suggests that the less nonradiative emission in the trapezoidal NPs. Figure 5c shows the TRPL spectroscopy of the two NPs, which could be well fitted by a biexponential function corresponding to nonradiative recombination channel with short

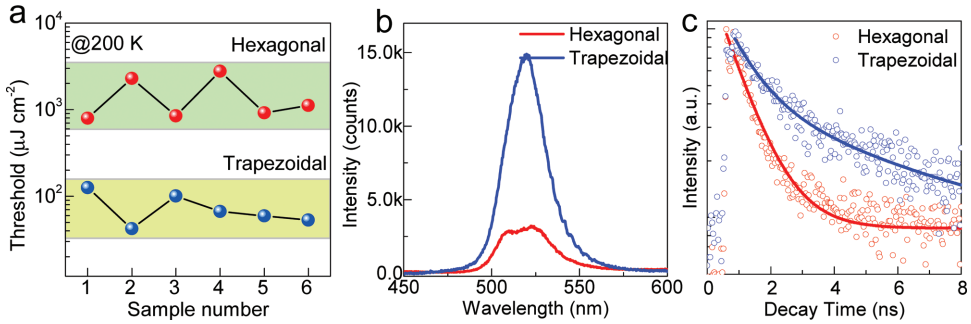

Figure 5. a) The lasing threshold comparison between the out-of-plane-epitaxial trapezoidal PbI_2 NPs (blue dots); in-plane-epitaxial hexagonal PbI_2 NPs (red dots). The temperature is 200 K. b) Room-temperature steady state PL spectra of the out-of-plane-epitaxial trapezoidal PbI_2 NPs (blue) and in-plane-epitaxial hexagonal PbI_2 NPs (red). The thickness of the NPs is ≈175 nm. c) The normalized TRPL spectra of out-of-plane-epitaxial trapezoidal PbI_2 NPs (blue) and in-plane-epitaxial hexagonal PbI_2 NPs (red) in (b). The TRPL can be well fitted by biexponential function.

lifetime and longer lifetime for radiative recombination. In trapezoidal NPs, the τ_{nr} and τ_r (0.86 and 4.78 ns) are longer than those of hexagonal NPs (τ_{nr}: 0.50 ns; τ_r: 3.79 ns), respectively, which is good consistent with the steady-state PL spectroscopy. The relatively longer nonradiative decay rate of the trapezoidal NPs, suggests less density of defect states and higher optical gain which then leads to lower lasing threshold.[76] Similar results are observed in the other NPs with different thicknesses (Figure S13, Supporting Information). Further, the absorption tail of trapezoidal NP is shorter than the hexagonal NP (Figure S14), strongly supporting that the trapezoidal NPs own better crystalline quality than the hexagonal NPs.

In summary, we have demonstrated the synthesis of trapezoidal PbI_2 NPs on mica substrate using incommensurate vdW epitaxy method. Low threshold FP lasing is demonstrated at 120–200 K due to population inversion of $n = 1$ exciton with threshold nearly one-order lower than previous studies. The superior lasing performance is ascribed to the slow nonradiative recombination rate owing to good crystalline quality of the NPs. These trapezoidal PbI_2 NPs would be potential for planar lasers and other 2D layered related optoelectronic applications.

Experimental Section

PbI_2 NPs Synthesis: Lead iodide powders (Aldrich, 99.999%) were used as the reaction source and placed into a single zone furnace quartz tube (OTF-1200X). A fresh cleaved muscovite mica substrate (2×4 cm^2) were placed in the downstream region inside the quartz tube. The quartz tube was then evacuated to a base pressure of 5×10^{-3} Torr followed by a 30 sccm flow of high-purity N_2. The growth temperature was 380 °C and the heating rate was 10 °C min^{-1}. The growth pressure and time was 200 Torr and 20 min, respectively.

Steady State and Time-Resolved PL Spectroscopy: For the steady-state PL spectra experiment, a CW 405 nm solid state laser was focused onto the samples by a 100× objective lens. The PL signal was collected by the same objective lens and analyzed by a monochromator equipped with charge coupled device (CCD) detector. A 407 nm long pass filter was adopted to block the excitation laser line. For the lasing characterization, the excitation source was femtosecond pulsed laser with wavelength of 400 nm which was doubled from the Coherent Libra regenerative amplifier (150 fs, 1 kHz, 800 nm). The pump laser was focused onto samples by a 50× objective and the diameter of the laser spot was ≈30 µm. To obtain the lasing images of the sample, the PL emission signals were imaged on a CCD camera using a long-pass filter to block the laser line. The HRTEM images and SAED patterns were acquired at a field-emission high resolution transmission electron microscope (Tecnai F30).

Supporting Information

Supporting Information is available from the Wiley Online Library or from the author.

Acknowledgements

Y.G.Z., Q.W., and Z.L. contributed equally to this work. Q.Z. acknowledges funding support from the Ministry of Science and Technology (2017YFA0304600 and 2017YFA0205700) and Natural Science Foundation of China (Nos. 61774003, 51502007, and 51672007). Q.Z. also thanks the support of start-up funding from Peking University, one-thousand talent programs from Chinese government, open research fund program of the state key laboratory of low-dimensional quantum physics. X.F.L. thanks the support from the Ministry of Science and Technology (Nos. 2016YFA0200700 and 2017YFA0205004), National Natural Science Foundation of China (No. 21673054), Key Research Program of Frontier Science, CAS (No. QYZDB-SSW-SYS031). G.C.X. acknowledges the financial support from Macau Science and Technology Development Fund (FDCT-116/2016/A3 and FDCT-091/2017/A2), Research Grant (SRG2016-00087-FST and MYRG2018-00148-IAPME) from University of Macau. P.G. thanks the support from "2011 Program" Peking-Tsinghua-IOP Collaborative Innovation Center of Quantum Matter. The authors would like to thank Prof. Q. Wang and Dr. Y. G. Guo for their fruitful suggestions.

Conflict of Interest

The authors declare no conflict of interest.

Keywords

layered semiconductor, microcavity, PbI_2, small laser, van der Waals epitaxy

Received: May 21, 2018
Revised: July 9, 2018
Published online: July 31, 2018

[1] Y. Gong, J. Lin, X. Wang, G. Shi, S. Lei, Z. Lin, X. Zou, G. Ye, R. Vajtai, B. I. Yakobson, *Nat. Mater.* **2014**, *13*, 1135.
[2] B. Radisavljevic, A. Radenovic, J. Brivio, i. V. Giacometti, A. Kis, *Nat. Nanotechnol.* **2011**, *6*, 147.
[3] O. Lopez-Sanchez, D. Lembke, M. Kayci, A. Radenovic, A. Kis, *Nat. Nanotechnol.* **2013**, *8*, 497.
[4] S. Wu, J. S. Ross, G.-B. Liu, G. Aivazian, A. Jones, Z. Fei, W. Zhu, D. Xiao, W. Yao, D. Cobden, *Nat. Phys.* **2013**, *9*, 149.
[5] R. Cheng, Y. Wen, L. Yin, F. Wang, F. Wang, K. Liu, T. A. Shifa, J. Li, C. Jiang, Z. Wang, *Adv. Mater.* **2017**, *29*, 1703122.
[6] F. Wang, Z. Wang, T. A. Shifa, Y. Wen, F. Wang, X. Zhan, Q. Wang, K. Xu, Y. Huang, L. Yin, *Adv. Funct. Mater.* **2017**, *27*, 1603254.
[7] R. Lv, J. A. Robinson, R. E. Schaak, D. Sun, Y. Sun, T. E. Mallouk, M. Terrones, *Acc. Chem. Res.* **2015**, *48*, 56.
[8] M. C. Gather, S. H. Yun, *Nat. Photonics* **2011**, *5*, 406.
[9] T.-i. Kim, J. G. McCall, Y. H. Jung, X. Huang, E. R. Siuda, Y. Li, J. Song, Y. M. Song, H. A. Pao, R.-H. Kim, *Science* **2013**, *340*, 211.
[10] W. Bogaerts, P. De Heyn, T. Van Vaerenbergh, K. De Vos, S. Kumar Selvaraja, T. Claes, P. Dumon, P. Bienstman, D. Van Thourhout, R. Baets, *Laser Photonics Rev.* **2012**, *6*, 47.
[11] P.-A. Blanche, A. Bablumian, R. Voorakaranam, C. Christenson, W. Lin, T. Gu, D. Flores, P. Wang, W.-Y. Hsieh, M. Kathaperumal, *Nature* **2010**, *468*, 80.
[12] J. C. Johnson, H.-J. Choi, K. P. Knutsen, R. D. Schaller, P. Yang, R. J. Saykally, *Nat. Mater.* **2002**, *1*, 106.
[13] M. H. Huang, S. Mao, H. Feick, H. Yan, Y. Wu, H. Kind, E. Weber, R. Russo, P. Yang, *Science* **2001**, *292*, 1897.
[14] Y. Liu, N. O. Weiss, X. Duan, H.-C. Cheng, Y. Huang, X. Duan, *Nat. Rev. Mater.* **2016**, *1*, 16042.
[15] M. J. Bowers, J. R. McBride, S. J. Rosenthal, *J. Am. Chem. Soc.* **2005**, *127*, 15378.
[16] H. Deng, G. Weihs, D. Snoke, J. Bloch, Y. Yamamoto, *Proc. Natl. Acad. Sci. USA* **2003**, *100*, 15318.
[17] S. Christopoulos, G. B. H. Von Högersthal, A. Grundy, P. Lagoudakis, A. Kavokin, J. Baumberg, G. Christmann, R. Butté, E. Feltin, J.-F. Carlin, *Phys. Rev. Lett.* **2007**, *98*, 126405.

[18] K. F. Mak, J. Shan, *Nat. Photonics* **2016**, *10*, 216.
[19] H. Zhu, Y. Fu, F. Meng, X. Wu, Z. Gong, Q. Ding, M. V. Gustafsson, M. T. Trinh, S. Jin, X. Zhu, *Nat. Mater.* **2015**, *14*, 636.
[20] M. Imada, S. Noda, A. Chutinan, T. Tokuda, M. Murata, G. Sasaki, *Appl. Phys. Lett.* **1999**, *75*, 316.
[21] Y. Ye, Z. J. Wong, X. Lu, X. Ni, H. Zhu, X. Chen, Y. Wang, X. Zhang, *Nat. Photonics* **2015**, *9*, 733.
[22] M. Gao, X. Zhang, B. Yang, J. Shen, *J. Chem. Soc., Chem. Commun.* **1994**, 2229.
[23] A. S. Toulouse, B. P. Isaacoff, G. Shi, M. Matuchová, E. Kioupakis, R. Merlin, *Phys. Rev. B* **2015**, *91*, 165308.
[24] I. Baltog, M. Baibarac, S. Lefrant, *J. Phys.: Conden. Matter* **2009**, *21*, 025507.
[25] A. Ferreira da Silva, N. Veissid, C. An, I. Pepe, N. Barros de Oliveira, A. Batista da Silva, *Appl. Phys. Lett.* **1996**, *69*, 1930.
[26] X. Zhu, Z. Wei, Y. Jin, A. Xiang, *Cryst. Res. Technol.* **2007**, *42*, 456.
[27] B. D. Milbrath, A. J. Peurrung, M. Bliss, W. J. Weber, *J. Mater. Res.* **2008**, *23*, 2561.
[28] J. Liu, Y. Zhang, *Cryst. Res. Technol.* **2017**, *52*, 1600370.
[29] Q. Zhang, S. T. Ha, X. Liu, T. C. Sum, Q. Xiong, *Nano Lett.* **2014**, *14*, 5995.
[30] Q. Zhang, R. Su, X. Liu, J. Xing, T. C. Sum, Q. Xiong, *Adv. Funct. Mater.* **2016**, *26*, 6238.
[31] S. T. Ha, X. Liu, Q. Zhang, D. Giovanni, T. C. Sum, Q. Xiong, *Adv. Opt. Mater.* **2014**, *2*, 838.
[32] R. Su, C. Diederichs, J. Wang, T. C. H. Liew, J. Zhao, S. Liu, W. Xu, Z. Chen, Q. Xiong, *Nano Lett.* **2017**, *17*, 3982.
[33] Q. Shang, S. Zhang, Z. Liu, J. Chen, P. Yang, C. Li, W. Li, Y. Zhang, Q. Xiong, X. Liu, Q. Zhang, *Nano Lett.* **2018**, *18*, 3335.
[34] S. Zhang, Q. Shang, W. Du, J. Shi, Z. Wu, Y. Mi, J. Chen, F. Liu, Y. Li, M. Liu, Q. Zhang, X. Liu, *Adv. Opt. Mater.* **2018**, *6*, 1701032.
[35] W. Du, S. Zhang, J. Shi, J. Chen, Z. Wu, Y. Mi, Z. Liu, Y. Li, X. Sui, R. Wang, X. Qiu, T. Wu, Y. Xiao, Q. Zhang, X. Liu, *ACS Photonics* **2018**, *5*, 2051.
[36] M. S. Brodin, I. Blonskyi, A. A. Dobrovolskii, V. N. Karataev, A. A. Kipen, *Laser Action in PbI_2 Layered Single Crystals*, Vol. *13*, Kvantovaya Elektronika, Russia **1986**.
[37] X. Liu, S. T. Ha, Q. Zhang, M. de la Mata, C. Magen, J. Arbiol, T. C. Sum, Q. Xiong, *ACS Nano* **2015**, *9*, 687.
[38] E. Doni, G. Grosso, G. Harbeke, E. Meier, E. Tosatti, *Phys. Status Solidi B* **1975**, *68*, 569.
[39] S. Steinberg, W. Ducker, G. Vigil, C. Hyukjin, C. Frank, M. Tseng, D. Clarke, J. Israelachvili, *Science* **1993**, *260*, 656.
[40] M. I. B. Utama, F. J. Belarre, C. Magen, B. Peng, J. Arbiol, Q. Xiong, *Nano Lett.* **2012**, *12*, 2146.
[41] X. Liu, Q. Zhang, Q. Xiong, T. C. Sum, *Nano Lett.* **2013**, *13*, 1080.
[42] M. Zhong, S. Zhang, L. Huang, J. You, Z. Wei, X. Liu, J. Li, *Nanoscale* **2017**, *9*, 3736.
[43] G. K. Kasi, N. R. Dollahon, T. S. Ahmadi, *J. Phys. D: Appl. Phys.* **2007**, *40*, 1778.
[44] Q. Zhang, J. Zhang, M. I. B. Utama, B. Peng, M. de la Mata, J. Arbiol, Q. Xiong, *Phys. Rev. B* **2012**, *85*.
[45] M. Y. Khilji, W. F. Sherman, G. R. Wilkinson, *J. Raman Spectrosc.* **1982**, *13*, 127.
[46] J. J. Lifson S, *J. Chem. Phys.* **1962**, *57*, 1137.
[47] Z. R. Dai, Z. W. Pan, Z. L. Wang, *Adv. Funct. Mater.* **2003**, *13*, 9.
[48] Z. R. Dai, Z. W. Pan, Z. L. Wang, *Solid State Commun.* **2001**, *118*, 351.
[49] C. Cong, J. Shang, L. Niu, L. Wu, Y. Chen, C. Zou, S. Feng, Z. J. Qiu, L. Hu, P. Tian, *Adv. Opt. Mater.* **2017**, *5*, 1700609.
[50] R. Frisenda, J. O. Island, J. L. Lado, E. Giovanelli, P. Gant, P. Nagler, S. Bange, J. M. Lupton, C. Schüller, A. J. Molina-Mendoza, *Nanotechnology* **2017**, *28*, 455703.
[51] Y. Wang, Y.-Y. Sun, S. Zhang, T.-M. Lu, J. Shi, *Appl. Phys. Lett.* **2016**, *108*, 013105.
[52] M. Zhong, L. Huang, H.-X. Deng, X. Wang, B. Li, Z. Wei, J. Li, *J. Mater. Chem. C* **2016**, *4*, 6492.
[53] T. Fukuma, Y. Ueda, S. Yoshioka, H. Asakawa, *Phys. Rev. Lett.* **2010**, *104*, 016101.
[54] P. A. Beckmann, *Cryst, Res. Technol.* **2010**, *45*, 455.
[55] A. Kojima, M. Ikegami, K. Teshima, T. Miyasaka, *Chem. Lett.* **2012**, *41*, 397.
[56] Y. P. Varshni, *Physica* **1967**, *34*, 149.
[57] N. Preda, L. Mihut, M. Baibarac, I. Baltog, S. Lefrant, *J. Phys.: Condens. Matter* **2006**, *18*, 8899.
[58] M. Baibarac, N. Preda, L. Mihut, I. Baltog, S. Lefrant, J. Y. Mevellec, *J. Phys.: Condens. Matter* **2004**, *16*, 2345.
[59] F. Riccardo, O. I. Joshua, L. L. Jose, G. Emerson, G. Patricia, N. Philipp, B. Sebastian, M. L. John, S. Christian, J. M.-M. Aday, A. Lucia, F. Michael, K. Tobias, N. Miguel Angel, L. David Perez de, M. P. Emilio, F.-R. Joaquín, C.-G. Andres, *Nanotechnology* **2017**, *28*, 455703.
[60] F. Levy, A. Mercier, J.-P. Voitchovsky, *Solid State Commun.* **1974**, *15*, 819.
[61] I. Dag, E. Lifshitz, *J. Phys. Chem.* **1996**, *100*, 8962.
[62] T. Schmidt, K. Lischka, W. Zulehner, *Phys. Rev. B* **1992**, *45*, 8989.
[63] D. Y. Qiu, F. H. da Jornada, S. G. Louie, *Phys. Rev. Lett.* **2013**, *111*, 216805.
[64] M. Ando, M. Yazaki, I. Katayama, H. Ichida, S. Wakaiki, Y. Kanematsu, J. Takeda, *Phys. Rev. B* **2012**, *86*, 155206.
[65] S. G. Elkomoss, A. S. Amer, *Phys. Rev. B* **1975**, *11*, 2222.
[66] G. Dresselhaus, *J. Phys. Chem. Solids* **1956**, *1*, 14.
[67] G. L. Sewell, *Philos. Mag.* **1958**, *3*, 1361.
[68] D. Yarkony, R. Silbey, *J. Chem. Phys.* **1976**, *65*, 1042.
[69] Y. Wang, X. Li, X. Zhao, L. Xiao, H. Zeng, H. Sun, *Nano Lett.* **2016**, *16*, 448.
[70] A. Ohtomo, K. Tamura, M. Kawasaki, T. Makino, Y. Segawa, Z. Tang, G. Wong, Y. Matsumoto, H. Koinuma, *Appl. Phys. Lett.* **2000**, *77*, 2204.
[71] T. Honda, H. Kawanishi, T. Sakaguchi, F. Koyama, K. Iga, *MRS Internet J. Nitride Semicond. Res.* **1999**, *4*, 548.
[72] M. S. Brodin, I. Blonskiĭ, A. Dobrovol'skiĭ, V. Karataev, N. Yanushevskiĭ, *Sov. J. Quantum Electron.* **1986**, *16*, 140.
[73] C.-X. Sheng, Y. Zhai, E. Olejnik, C. Zhang, D. Sun, Z. V. Vardeny, *Opt. Mater. Exp.* **2015**, *5*, 530.
[74] A. M. Stoneham, *Rep. Prog. Phys.* **1981**, *44*, 1251.
[75] D. Y. Kondakov, J. R. Sandifer, C. W. Tang, R. H. Young, *J. Appl. Phys.* **2003**, *93*, 1108.
[76] F. Wu, J. Z. Zhang, R. Kho, R. K. Mehra, *Chem. Phys. Lett.* **2000**, *330*, 237.